Temperature dependence of phonons in $FeGe_2$

Hillary L. Smith,[1,*,†] Yang Shen,[1,*,‡] Dennis S. Kim,[1] Fred C. Yang,[1] C. P. Adams,[2] Chen W. Li,[3] D. L. Abernathy,[4] M. B. Stone,[4] and B. Fultz[1,§]

[1]*Department of Applied Physics and Materials Science, California Institute of Technology, Pasadena, California 91125, USA*

[2]*Department of Physics, St. Francis Xavier University, Antigonish, Nova Scotia, Canada B2G 2W5*

[3]*Department of Mechanical Engineering and Materials Science and Engineering, University of California, Riverside, Riverside, California 92521, USA*

[4]*Oak Ridge National Laboratory, Neutron Scattering Division, Oak Ridge, Tennessee 37831, USA*

(Received 25 November 2017; revised manuscript received 5 August 2018; published 9 October 2018)

Inelastic neutron scattering was used to measure phonon dispersions in a single crystal of $FeGe_2$ with the C16 structure at 300, 500, and 635 K. Phonon densities of states (DOS) were also measured on polycrystalline $FeGe_2$ from 325 to 1050 K, and the Fe partial DOS was obtained from polycrystalline $^{57}FeGe_2$ at 300 K using nuclear resonant inelastic x-ray scattering. The dominant feature in the temperature dependence of the phonon spectrum is thermal broadening of high-energy modes. The energy shifts of the low- and high-energy parts of the spectrum were almost the same. DFT calculations performed with the quasiharmonic approximation gave results in moderate agreement with the experimental thermal energy shifts, although the isobaric Grüneisen parameter calculated from the quasiharmonic model was smaller than that from measurements. The thermal broadening of the phonon spectrum and dispersions, especially at high energies, indicates a cubic anharmonicity to second order that should also induce phonon shifts. We show that different anharmonic contributions cancel out, giving average phonon shifts in moderate agreement to calculations with the quasiharmonic approximation. The different parts of the large phonon contribution to the entropy are separated for $FeGe_2$, showing modest but interpretable anharmonic contributions.

DOI: 10.1103/PhysRevMaterials.2.103602

I. INTRODUCTION

Germanium-based alloys are of interest for applications in spin-based electronic devices [1]. Beginning in 1961 [2], $FeGe_2$ has been the focus of numerous experimental and theoretical studies to describe its magnetic properties [3–9]. This material exhibits two zero-field magnetic phase transitions at temperatures of $T_N = 289$ K and $T_c = 263$ K. The first transition corresponds to a second-order Néel transition from a paramagnetic high-temperature phase to an incommensurate spin-density-wave state (intermediate-temperature phase, ITP). The second transition corresponds to a first-order transition to the antiferromagnetic low-temperature phase [8]. The phonon properties of $FeGe_2$ have received less attention but provide an excellent opportunity to determine how well the thermodynamic functions of anharmonic materials can be understood.

$FeGe_2$ has the same body-centered tetragonal C16 crystal structure [10] (see Fig. 1) as θ-phase Al_2Cu, in which an anomalously large vibrational entropy was reported by Wolverton and Ozoliņš [11]. The calculated electronic energy of the equilibrium θ phase (C16 structure) was found to be 15 meV/atom larger than that of the θ_c' phase (C1 fluorite structure). The authors concluded that the θ phase is stabilized at finite temperature by vibrational entropy, and this entropic stabilization of the θ phase may originate with features of its low-symmetry structure.

$FeGe_2$ is also a likely candidate for large phonon anharmonicity related to phonon-phonon interactions because of the absence of inversion symmetry at Ge atoms [12]. The phonon energies can have a temperature dependence from a number of competing mechanisms beyond the harmonic or quasiharmonic approximations, as observed in other transition-metal systems [13].

Here we report results from a combined experimental and computational study on the phonon dynamics of $FeGe_2$. Phonon dispersions and phonon density of states (DOS) were measured by inelastic neutron scattering (INS), and Fe partial DOS were measured by nuclear resonant inelastic x-ray scattering (NRIXS). First-principles calculations based on density functional theory (DFT) with the quasiharmonic approximation (QHA) were performed between 325 and 1050 K, and the small-displacement method was used to calculate the phonons. Separately, a fully anharmonic calculation was performed at 635 K using the stochastically initialized temperature-dependent effective potential method (s-TDEP) [14]. The DFT calculations with QHA, which only consider the volume expansion without thermal effects, are in close agreement with the phonon DOS data in the low-energy region, but discrepancies between the QHA calculations and the experimental data are found in the high-energy region, indicating a strong anharmonicity of the high-energy phonon

*These authors contributed equally to this work.
†hls@caltech.edu
‡yshen@caltech.edu
§btf@caltech.edu

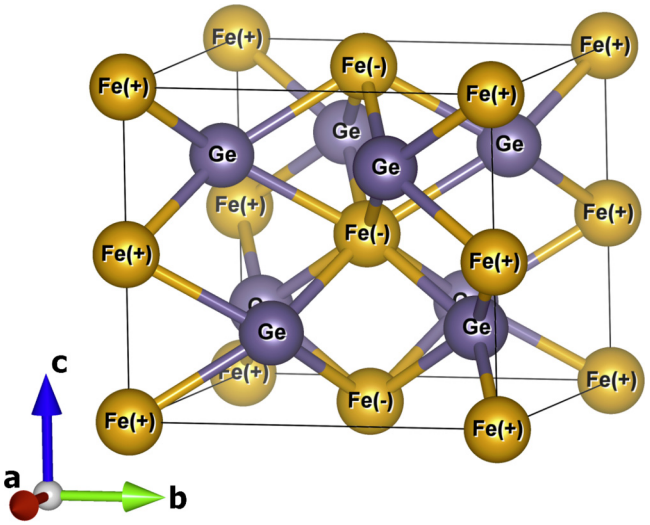

FIG. 1. Crystal structure of $FeGe_2$. It is a tetragonal C16 structure with alternating layers of Fe and Ge atoms. The positions of atoms are [4]: Fe (orange) at $(0,0,0)$, $(0,0,\frac{1}{2})$ and Ge (blue) at $(x,\frac{1}{2}+x,\frac{1}{4})$, $(\bar{x},\frac{1}{2}-x,\frac{1}{4})$, $(\frac{1}{2}+x,\bar{x},\frac{1}{4})$, $(\frac{1}{2}-x,x,\frac{1}{4})$, where $x=0.1547$ is the atomic parameter for Ge positions. Bonds are only drawn between first nearest neighborhoods (1NN). Plus and minus signs identify the collinear spin structure of the antiferromagnetic low-temperature phase [3–9].

modes. The difference between the calculated and measured isobaric Grüneisen parameter shows that the QHA alone is insufficient to model the softening of individual phonons with temperature, even though the average behavior is semiquantitatively correct.

II. EXPERIMENT

The sample of $FeGe_2$ was a semicylindrical crystal 15 mm in radius and 40 mm in length with a mass of 110 g. This crystal was loaned from Oak Ridge National Laboratory and previously measured by Adams *et al.* [9]. Polycrystalline samples of $FeGe_2$ were prepared from a mixture of the elements of 99.99% purity by arc-melting in a Ti-gettered argon atmosphere, followed by annealing under vacuum. Samples at isotopically enriched $^{57}FeGe_2$ were prepared similarly.

INS measurements were performed on both single-crystal and powder samples with the time-of-flight Wide Angular-Range Chopper Spectrometer, ARCS, at the Spallation Neutron Source at Oak Ridge National Laboratory. An incident energy of 70 meV was used for all measurements. The powder sample was placed in a Nb foil sachet and mounted in a low-background electrical resistance vacuum furnace for measurements at temperatures of 325, 476, 650, 850, and 1050 K. The lattice constants were obtained from elastic scattering, acquired simultaneously, and integrated over a range of ± 1 meV. The single crystal was mounted inside the same furnace with the $[HK0]$ crystallographic plane horizontal, and measurements were performed at 300, 500, and 635 K.

Data reduction was performed with MANTID [15]. The single-crystal and powder data were normalized by the proton current on target. Bad detector pixels were identified and masked, and the data were corrected for detector efficiency using a measurement from vanadium. The phonon DOS curves from powder data were obtained after corrections for multiphonon and multiple scattering using the GETDOS package [16]. The single-crystal neutron data from 240 rotations in increments of 0.5° about the vertical axis were reduced to create the four-dimensional $S(\mathbf{Q},E)$. Single-crystal data analysis was performed with DAVE [17].

NRIXS measurements were performed on the $^{57}FeGe_2$ at beamline 16ID-D at the Advanced Photon Source at Argonne National Laboratory [18,19]. The powder sample was secured in Kapton tape and placed at a grazing angle to the incident x-ray beam. Incoherently reradiated photons were measured by two avalanche photodiode detectors (APD) positioned normal to the incident beam. The energy was scanned from -160 to $+160$ meV around the nuclear resonance energy of ^{57}Fe 14.413 keV. Several scans were combined for final analysis. The energy resolution of all NRIXS measurements was measured to be 2.1858 meV (FWHM) at the elastic line. NRIXS data was reduced using the PHOENIX code [20].

III. COMPUTATION

The *ab initio* DFT calculations were performed with the VASP package [21–23] on a plane-wave basis set, using the projector augmented wave (PAW) pseudopotentials [24] with the Perdew-Burke-Ernzerhof (PBE) exchange-correlation functional [25]. The energy cutoff was 600 eV for all calculations. The phonon DOS with QHA was calculated on a supercell of 216 atoms with a $2\times2\times2$ k-point mesh using the small-displacement method as implemented in the PHONOPY code [26]. Except for the ground states discussed in Sec. V A, all the phonon-related calculations are non-spin-polarized.

The QHA for phonon behavior was obtained from the thermal expansion at elevated temperatures using lattice parameters obtained from the neutron scattering experiments. The neutron weighting arising from the efficiency for phonon scattering of neutrons by different modes was taken into consideration when comparing the computations with the experimental results. For $FeGe_2$, the neutron-weighted DOS [27] is

$$g^{\mathrm{NW}}(\epsilon) = A^{-1}\sum_i g_i(\epsilon)\frac{\sigma_{sc,i}}{m_i}x_i \simeq 0.47 g_{\mathrm{Fe}}(\epsilon) + 0.53 g_{\mathrm{Ge}}(\epsilon), \quad (1)$$

where $g_i(\epsilon)$ is the phonon partial DOS of atom i (i.e., Fe pDOS or Ge pDOS), $\sigma_{sc,i}$ is the total scattering cross section, m_i is the atomic mass, x_i is the mole fraction, and A is a normalization factor.

Beyond the QHA, the finite-temperature phonons at 635 K were calculated with the s-TDEP method [28–30]. In this procedure, the Born-Oppenheimer surface of $FeGe_2$ at 635 K was sampled by a Monte Carlo sampling of atomic positions and momentum near equilibrium positions. By using DFT with various configurations of displaced atoms by a stochastic sampling of a canonical ensemble, with Cartesian displacements (u_i^α) normally distributed around the mean thermal displacement, the forces on atoms were fitted to a model

Hamiltonian,

$$\hat{H} = U_0 + \sum_i \frac{\mathbf{p}_i^2}{2m_i} + \frac{1}{2!}\sum_{ij}\sum_{\alpha\beta}\Phi_{ij}^{\alpha\beta}u_i^\alpha u_j^\beta + \frac{1}{3!}\sum_{ijk}\sum_{\alpha\beta\gamma}\Phi_{ijk}^{\alpha\beta\gamma}u_i^\alpha u_j^\beta u_k^\gamma \ldots, \quad (2)$$

Here, U_0 is a fit parameter for the baseline of the potential energy surface. The quadratic force constants Φ_{ij} from the thermally displaced atoms capture not only harmonic properties but also temperature-dependent nonharmonic effects, and are used to calculate phonon frequencies. The cubic force constants Φ_{ijk} capture phonon-phonon interactions (PPI) that contribute to the broadening and additional shifts of phonon modes. For first-principle force constant calculations, the supercell of a $2 \times 2 \times 3$ conventional unit cell with 144 atoms was used with a $3 \times 3 \times 2$ Monkhorst-Pack k-point grid and a plane-wave energy cutoff of 650 eV. The exchange-correlation energy was also calculated with the PBE functional.

From many-body interactions, the temperature-dependent renormalized phonon frequencies were corrected by calculated the linewidths Γ_λ and shifts Δ_λ arising from anharmonicity, or phonon-phonon interactions. This required the calculation of the real and imaginary parts of the phonon self-energy

$$\Sigma(\Omega) = \Delta(\Omega) + i\Gamma(\Omega), \quad (3)$$

where $\Omega(=E/\hbar)$ is the probing energy. Phonon lifetimes τ are related to the imaginary part of the self-energy by

$$1/\tau = 2\Gamma_\lambda, \quad (4)$$

for mode λ evaluated at the harmonic frequency. Given the third-order force constants, the imaginary part of the phonon self-energy can be calculated,

$$\Gamma_\lambda(\Omega) = \frac{\hbar\pi}{16}\sum_{\lambda'\lambda''}|\Phi_{\lambda\lambda'\lambda''}|^2\{(n_{\lambda'} + n_{\lambda''} + 1) \times \delta(\Omega - \omega_{\lambda'} - \omega_{\lambda''}) + (n_{\lambda'} - n_{\lambda''}) \times [\delta(\Omega - \omega_{\lambda'} + \omega_{\lambda''}) - \delta(\Omega + \omega_{\lambda'} - \omega_{\lambda''})]\}, \quad (5)$$

and the real component is obtained by a Kramers-Kronig transformation

$$\Delta(\Omega) = \mathcal{P}\int \frac{1}{\pi}\frac{\Gamma(\omega)}{\omega - \Omega}d\omega. \quad (6)$$

The imaginary component of the self-energy is a sum over all possible three-phonon interactions, where $\Phi_{\lambda\lambda'\lambda''}$ is the three-phonon matrix element determined from the cubic force constants Φ_{ijk} by the Fourier transform, n is the Bose-Einstein thermal occupation factors counting the number of phonons in each mode, and the δ functions conserve energy and momentum. Γ_λ and Δ_λ were calculated with a $16 \times 16 \times 16\,q$-grid.

Compared with the quasiharmonic (QH) model, this s-TDEP method includes higher-order phonon-phonon interactions at elevated temperatures by renormalizing terms in the model Hamiltonian, adding shifts (Δ_λ) of the frequencies perturbatively to the harmonic frequencies. It also reveals the phonon broadening from the imaginary part of the phonon self-energy, which is purely an anharmonic effect.

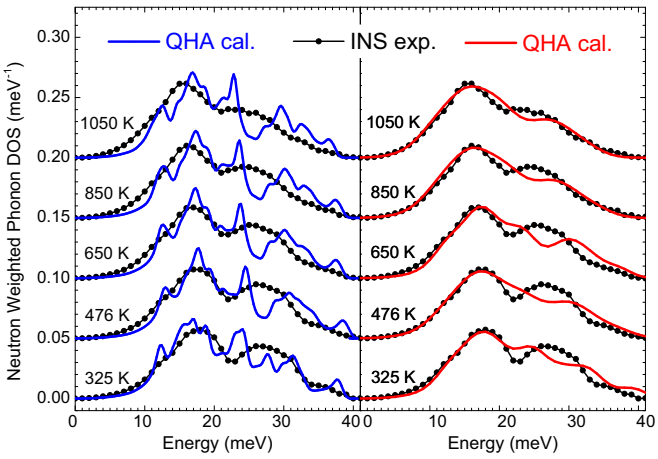

FIG. 2. Neutron-weighted phonon DOS of $FeGe_2$. Experimental data from INS (black circles) is overlaid with the DOS calculated with the quasiharmonic approximation (a, left) before convolution (blue line) and (b, right) after convolution (red line). Curves are normalized to unity and offset for clarity.

IV. RESULTS

Phonon DOS curves measured with INS are shown in Fig. 2 (black symbols). By fitting the two main DOS peaks to Lorentzian functions, the temperature dependences of the positions and linewidths of these peaks are shown in Fig. 3. They were fitted to linear functions, but the phonon broadening of the high-energy modes included a quadratic term. The low-energy and high-energy modes both soften similarly with temperature. However, the width of the low-energy modes shows little change with temperature, whereas the high-energy modes broaden superlinearly with temperature, indicating shorter phonon lifetimes.

Neutron powder diffraction patterns, obtained from integration of the elastic scattering from the powder samples, were analyzed to obtain lattice constants as a function of temperature. Linear thermal expansion of the lattice constants is observed, in agreement with previously reported room-temperature data [31]. Lattice parameters and coefficients of thermal expansion are reported in the Supplemental Material [32].

Using the experimental lattice constants, the phonon DOS of $FeGe_2$ was calculated with the quasiharmonic approximation as described in Sec. III. By applying the proper weights on the calculated pDOS using Eq. (1), and by the convolution with a Gaussian function approximating the instrument resolution, the simulated neutron-weighted phonon DOS was obtained as shown in Fig. 2(b) (red line). More details on the partial phonon DOS are shown in the Supplemental Material [32]. The calculated, neutron-weighted DOS curves are in good agreement with the experimental measurements in the low-energy region, but there is a noticeable discrepancy in the high-energy modes. The discrepancies become larger with temperature. This is shown more directly by the QHA-calculated phonon DOS before convolution in Fig. 2(a), though the discrepancies at high energies, including one gap and a few peaks above 21 meV, are smoothed out by the convolution [Fig. 2(b)].

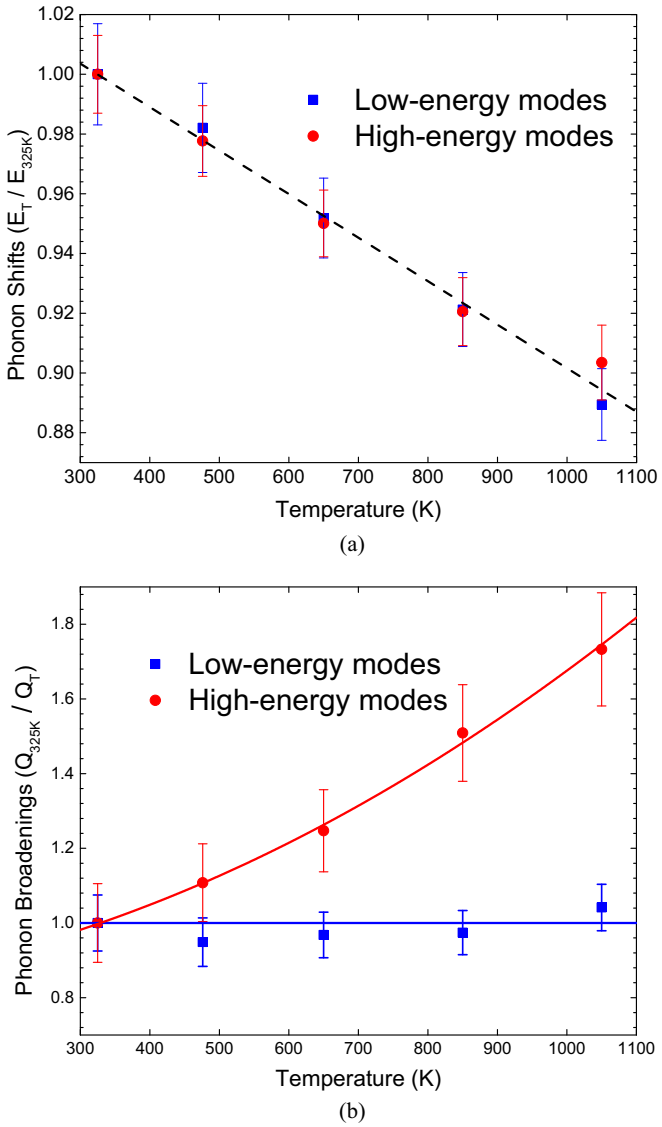

FIG. 3. Temperature dependence of phonon modes. (a) Phonon shifts and (b) phonon broadenings are shown as functions of temperature. The low- and high-energy modes refer to the two main peaks in the phonon DOS curves shown in Fig. 2. They are all linear with temperature, except for the phonon broadening of the high-energy modes. Error bars are from the fitting procedure.

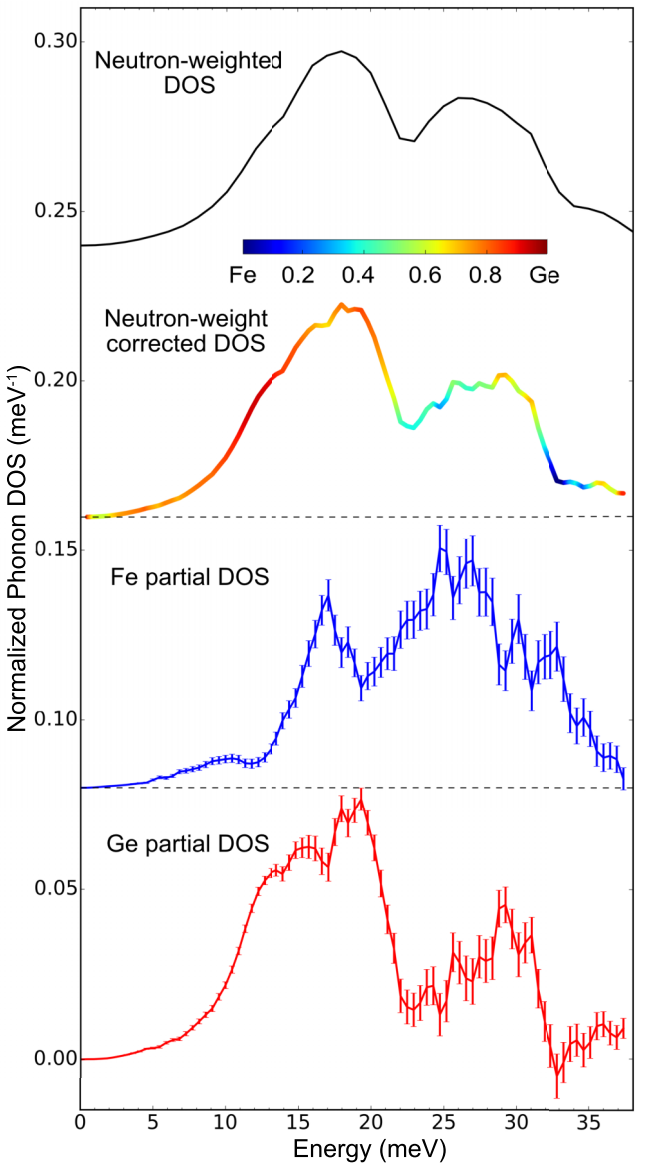

FIG. 4. Correcting the neutron weighting using Eq. (1) by measuring the Fe partial DOS from NRIXS experiments. All data are normalized to unity and at a temperature of 325 K. Error bars are from counting statistics.

The Fe partial DOS from NRIXS measurements at 325 K is shown in Fig. 4. Normalized NRIXS and INS data were used with Eq. (1) to obtain the Ge pDOS. The neutron-weight-corrected phonon DOS was then obtained at 325 K as shown in Fig. 4. It is found that neutron weighting has a negligible influence on the shapes of phonon DOS curves of $FeGe_2$, simplifying interpretations from the neutron-weighted phonon DOS curves at other temperatures.

Figure 5 shows phonon dispersions along the [100] direction at 300, 500, and 635 K (a–c). The gray stripe indicates the region at 4 r.l.u. (reciprocal lattice units), where a cut of intensity as a function of E is taken and shown in (d). Fits to the experimental data with Gaussian functions give the peak positions in (e). The shaded regions in (e) represent the FWHM of the fitted peak. The energy of the high-energy mode calculated with the QH approximation is also plotted in (e) in black. Figure 6 shows phonon dispersions along the [110] direction at 300, 500, and 635 K (a–c). Again, the gray strips indicate the positions of cuts along E that are shown in (d) and (f). The peak energies from Gaussian fits are shown in (e) and (g), with the peak energy from the QH approximation plotted in (g) in black. As is clear from the quasiharmonic DFT calculation overlaying the data in Fig. 7, there are many modes present. Acoustic modes can be identified, but their steep slope makes it difficult to see changes in them. As a result, Figs. 5(e) and 6(g) show a comparison between the data and the model for only the higher-energy optical modes.

The phonon dispersions are particularly informative for understanding the dynamic behavior of specific modes as a function of temperature. The phonon dispersions are analyzed

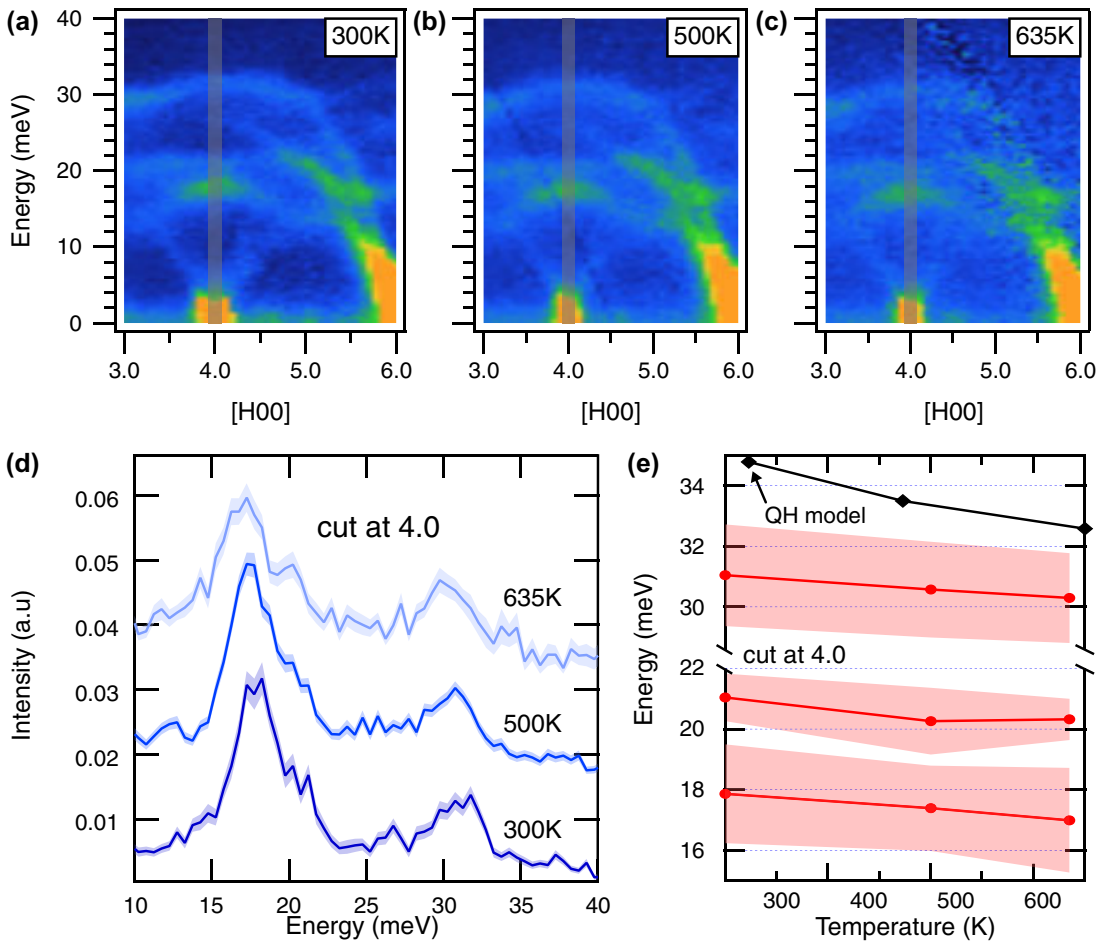

FIG. 5. Single-crystal $FeGe_2$ along the $[H00]$ direction. (a)–(c) The $[H00]$ direction at 300, 500, and 635 K, respectively. The gray stripe indicates the region of the cut shown in (d). (d) Cut of data at 4.0 r.l.u. is shown for 300 K (dark blue), 500 K (blue), and 635 K (light blue), offset for clarity, with error bars represented by the width of the curve. (e) Positions of low- and high-energy modes from fits to the experimental data in (d) are in red with the shaded region showing the linewidth approximated by the peak FWHM. The position of the high-energy mode predicted by the quasiharmonic model is shown in black.

at r.l.u. >2 to avoid spectral weight from magnon scattering. A closer inspection of the phonons along the [110] direction, shown in Fig. 6, shows several modes between 2 and 4.5 r.l.u., with the highest-energy mode near 31 meV. Both high-energy and low-energy modes show similar shifts with temperature, but the high-energy mode broadens more rapidly with temperature than the lower-energy mode, becoming more difficult to discern at 635 K. The phonons along the [100] direction (Fig. 5) show similar behavior. A distinctive low-energy band does not appear to broaden significantly with temperature but exhibits a similar thermal shift as the high-energy modes.

V. DISCUSSION

A. Stabilization of the ground state

The electronic energies of $FeGe_2$ were calculated for C16 and C1 (fluorite) crystal structures with nonmagnetic, ferromagnetic, and antiferromagnetic states. The minimum energies for each structure are listed in Table I. The ground state of $FeGe_2$ is found to be the C16 structure in the antiferromagnetic state. Magnetism decreases the ground-state energy of the C16 structure significantly compared to the nonmagnetic states—the energy of the antiferromagnetic state is about 9 meV/atom lower than the ferromagnetic state in the C16 structure, consistent with the calculations by Grechnev *et al.* [33].

B. Quasiharmonic approximation

The mode Grüneisen parameter is defined as

$$\gamma_i \equiv -\frac{V}{\epsilon_i}\frac{\partial \epsilon_i}{\partial V}, \tag{7}$$

where ϵ_i is the energy of phonon mode i, and a mean Grüneisen parameter $\bar{\gamma}$ averages the thermal behavior of all phonons in the Brillouin zone [34]:

$$\bar{\gamma} \equiv -\left\langle \frac{V}{\epsilon_i}\frac{\partial \epsilon_i}{\partial V} \right\rangle = -\left\langle \frac{\partial \ln \epsilon_i}{\partial \ln V} \right\rangle. \tag{8}$$

These two conventional Grüneisen parameters are used describe the phonon energy shifts with respect to volume, while the isobaric Grüneisen parameter $\bar{\gamma}_P(T)$ quantifies the

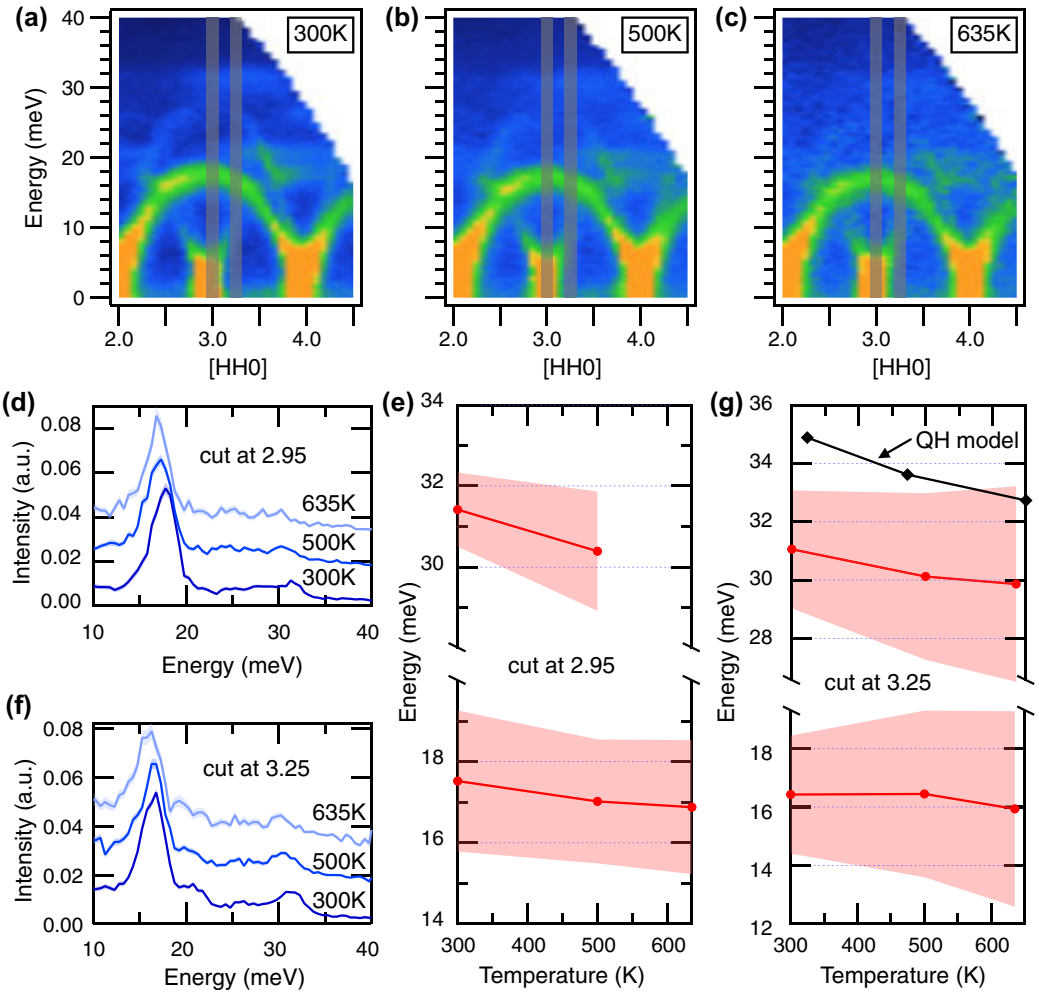

FIG. 6. Single-crystal $FeGe_2$ along the $[HH0]$ direction. (a)–(c) The $[HH0]$ direction at 300, 500, and 635 K, respectively. White spaces indicate regions without detector coverage. The gray stripes indicate the region of the cuts shown in (d) and (f). (d), (f) Cuts of data at 2.95 and 3.25 r.l.u., respectively, at 300 K (dark blue), 500 K (blue), and 635 K (light blue), offset for clarity, with error bars represented by the width of the curve. (e), (g) Positions of low- and high-energy modes from fits to the experimental data in (d) and (f), respectively, are shown in red. The shaded regions show the linewidth approximated by the peak FWHM. The position of the high-energy mode predicted by the QH model is shown in black.

temperature dependence of the phonon energy shifts,

$$\bar{\gamma}_P(T) \equiv -\frac{1}{3\alpha(T)}\left\langle \frac{\partial \ln \epsilon_i}{\partial T}\right\rangle\Big|_P. \tag{9}$$

A weighted average of the contributions from the low- and high-energy phonon modes [Eq. (10)] can be used to evaluate $\bar{\gamma}_P(T)$. The positions of the fitted peak centers were used to approximate the phonon mode energies in the low- and high-energy regions as

$$\begin{aligned}\bar{\gamma}_P^{\text{Exp.}}(T) &\simeq -\frac{1}{3\alpha(T)}\left\langle \sum_{i\in\text{low}} \frac{1}{\epsilon_i}\frac{\partial \epsilon_i}{\partial T} + \sum_{i\in\text{high}} \frac{1}{\epsilon_i}\frac{\partial \epsilon_i}{\partial T}\right\rangle\Big|_P \\ &\equiv \left\langle n_{\text{low}}\cdot \bar{\gamma}_{P,\text{low}}^{\text{Exp.}} + n_{\text{high}}\cdot \bar{\gamma}_{P,\text{high}}^{\text{Exp}}\right\rangle, \end{aligned}\tag{10}$$

where the weights, n_{low} and n_{high}, were from the areas under the two fitted Lorentzian functions as described at the beginning of Sec. IV.

The $\bar{\gamma}_P^{\text{Exp.}}$ was also obtained from the first moment of the phonon DOS curves,

$$\bar{\gamma}_P^{\text{Exp.}} = -\frac{1}{3\alpha(T)}\frac{1}{\bar{\epsilon}}\frac{\partial \bar{\epsilon}}{\partial T}\Big|_P, \tag{11}$$

where $\bar{\epsilon}$ is defined as

$$\bar{\epsilon} = \frac{\int \epsilon g(\epsilon) d\epsilon}{\int g(\epsilon) d\epsilon}. \tag{12}$$

Table II lists the Grüneisen parameters at 650 K from experiment and calculations with the quasiharmonic approximation. There is a non-negligible discrepancy between the experimental and calculated $\bar{\gamma}_P$, implying that the measured isobaric Grüneisen parameter of $FeGe_2$ contains contributions not only from the quasiharmonic model, which is a static volume-dependent approximation, but also from anharmonicity beyond the quasiharmonic model.

Measured phonon dispersion curves are shown along two crystallographic directions in Fig. 7, overlaid with dispersions

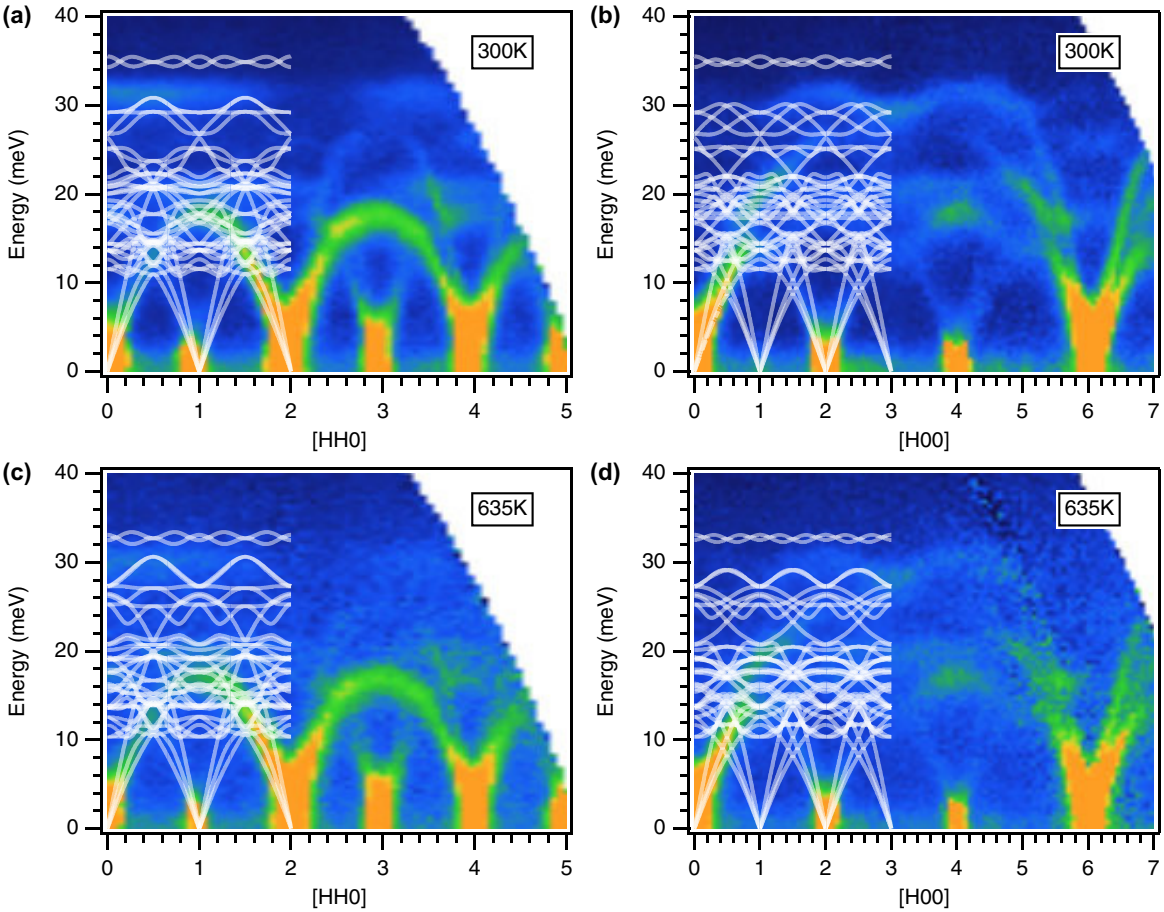

FIG. 7. Single-crystal $FeGe_2$ overlaid with QH calculation. Phonon dispersion curves from the QH calculation are mapped over the measured $S(\mathbf{Q}, E)$. The calculated dispersions are truncated for clarity but extend further in reciprocal lattice units with the same periodicity. (a), (b) The $[H\,H\,0]$ and $[H00]$ direction at 300 K, respectively. (c), (d) $[H\,H\,0]$ and $[H00]$ direction at 635 K, respectively.

calculated with the quasiharmonic approximation. The quasiharmonic predictions for the highest-energy phonon branches differ from the experimental results, perhaps owing to anharmonic effects or magnetic short-range order. The temperature dependences predicted by the quasiharmonic approximation are of the correct magnitude but are not accurate in detail. Similar discrepancies with the quasiharmonic approximation are found for high-energy phonon peaks in the energy cuts shown in Figs. 6(e) and 5(g). The quasiharmonic model predicts many low-energy phonon branches, some of which are in agreement with the experiment result. The large number of low-energy modes in $FeGe_2$ impedes the identification of the low-energy modes in Figs. 6(e) and 5(e), however. More analyses of phonon dispersions along additional crystallographic directions are given in the Supplemental Material [32].

TABLE I. Minimum energies for C16 and C1 structure, respectively, from DFT calculations for nonmagnetic, ferromagnetic (FM), and antiferromagnetic (AFM) states.

	Energy [eV/atom]		
Crystal structure	Nonmagnetic	FM	AFM
C16	–5.756	–5.798	–5.807
Fluorite	–5.680	–5.684	–5.688

C. Anharmonic behavior

To assess the importance of different contributions to phonon anharmonicity, consider their order with respect to the harmonic contribution $\Phi^{(2)}u^2$ (where Φ is a potential and u is a displacement):

$$\mathcal{O}(\Sigma) = \frac{\Phi^{(3')}}{\Phi^{(2)}}\,u + \frac{\Phi^{(4)}}{\Phi^{(2)}}\,u^2 + \left(\frac{\Phi^{(3)}}{\Phi^{(2)}}\right)^2 u^2 + \cdots, \quad (13)$$

TABLE II. Measured and calculated Grüneisen parameter of $FeGe_2$ at 650 K. The calculation used the quasiharmonic approximation. The experimental results were obtained from peak positions and the first moment of the measured phonon DOS curves, respectively.

	Calculation	Experiment			
$T = 650$ K	QHA model	From peak positions	Low-energy modes contribution	High-energy modes contribution	From $\bar{\epsilon}$
$\bar{\gamma}_P$	2.37	2.69	2.75	2.60	2.46

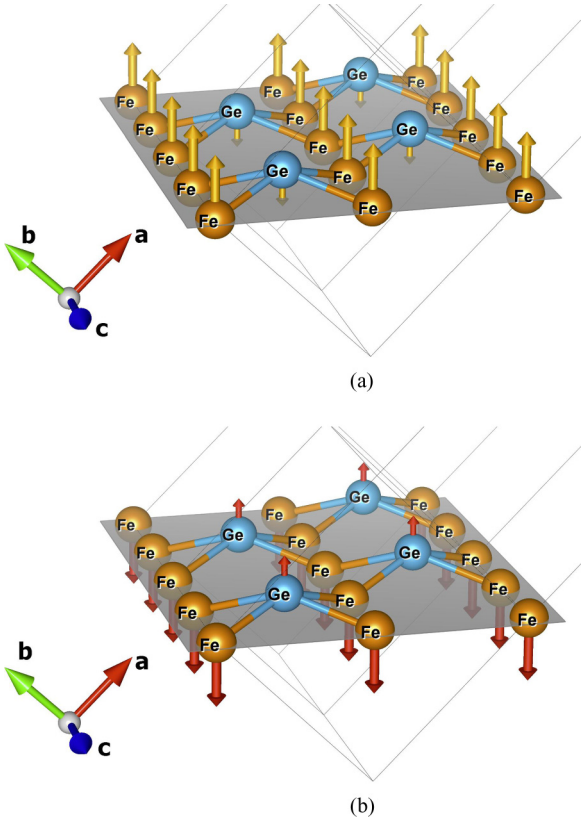

FIG. 8. Displacement pattern for LO phonons in the [110] direction. The Fe-Ge bonds undergo asymmetrical stretching when Fe (orange) and Ge (blue) atoms move towards (a, green arrows) and away from (b, red arrows) each other.

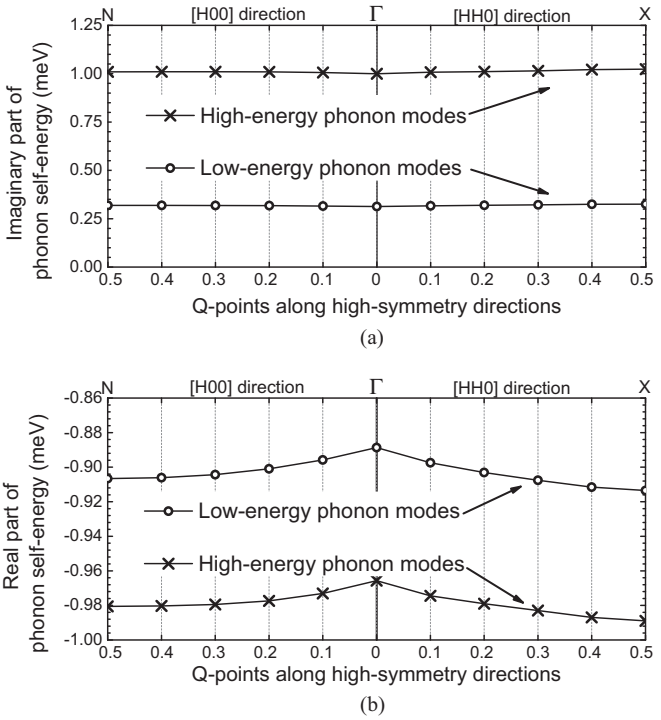

FIG. 9. Phonon self-energy of $FeGe_2$ along $[HH0]$ and $[H00]$ directions at 635 K. (a) Imaginary part of the phonon self-energy which gives the spectral linewidth. (b) Real part of the phonon self-energy which accounts for the phonon energy shifts. It is shown that the high-energy phonon modes (above 21 meV) have much shorter phonon lifetimes than the low-energy modes ($\Gamma_{\text{high}}/\Gamma_{\text{low}} \simeq 4$), while the softening in the high- and low-energy phonon modes is almost the same ($|(\Delta_{\text{high}} - \Delta_{\text{low}})/\Delta_{\text{high}}| \simeq 7.5\%$).

which shows the well-known result that the cubic term to second order [with $(\Phi^{(3)})^2$] is comparable to the quartic term. Equation (13) shows that the cubic term to first order (with $\Phi^{(3')}$) could dominate at small displacements. If the phonon potential is an even function of amplitude, this cubic term to first order is forbidden. In a low-symmetry C16 structure of $FeGe_2$, however, this first-order cubic term is allowed for some phonon modes. Its contribution to the phonon self-energy is real, and therefore contributes only to the energy shift and not to the broadening [12].

The experimental phonon DOS shows distinctly more broadening of the high-energy part of the spectrum. This could be caused by either lifetime broadenings of individual phonons, or to a distribution of phonon frequency shifts. Examinations of dispersions shown in this text, the Supplemental Material, and many others showed that the dominant thermal effect is the energy broadening of the high-energy phonon modes, although there is also a greater distribution of phonon frequency shifts at high energies than low. The lowest-order term in the phonon self-energy having an imaginary part is the cubic to second order [35], and this term is expected to dominate the lifetime broadening.

For a crystallographic site without inversion symmetry, a first-order cubic anharmonicity is possible and may be important for small displacements. Such a contribution is possible for the LO modes shown in Fig. 8 for the C16 structure. The phonon potential is not symmetric under inversion. For first-neighbor Fe-Ge bonds, the Fe-Ge bond length is different if Fe and Ge atoms are moving towards or away from each other, and the change in Fe-Ge bond length differs for the same displacements in the two directions. Anharmonicity of the Fe-Ge bonds is suggested by the measured partial phonon DOS curves. At 325 K, the discrepancy between the phonon modes in experiment and in the quasiharmonic model is greatest around 29 meV (Fig. 2). Around 29 meV, both Fe and Ge have a significant contribution to the total phonon DOS (Fig. 4).

For further study of the anharmonic behavior, the phonon spectrum function along $[HH0]$ and $[H00]$ directions at 635 K was investigated by *ab initio* DFT calculations with the stochastic temperature-dependent effective potential technique (sTDEP). Third-order force constants were used to calculate the imaginary and real part of the phonon self-energy. As shown in Fig. 9, they do not vary much. The imaginary part shows that the high-energy phonon modes (above ~21 meV) have much shorter phonon lifetimes than the low-energy phonon modes, which is indicated by Eq. (4), while the real part shows that their averaged energy shifts are almost the same. This is consistent with the results obtained from the phonon DOS measurements and single-crystal data. Beyond the QHA, the cubic anharmonicity plays an important role in the phonon broadening in the high-energy modes of $FeGe_2$. More details on the phonon spectral function and phonon

self-energy at specific Q points along these two directions can be found in the Supplemental Material [32].

D. Heat capacity and entropy

Figure 10 shows the temperature dependence of the thermal properties of $FeGe_2$. The phonon entropy S_{ph} was obtained from the phonon DOS $g(E)$ by

$$S_{ph} = 3k_B \int dE g(E)[(n+1)\ln(n+1) - n\ln n], \quad (14)$$

where n is the Planck distribution at temperature T,

$$n = \frac{1}{e^{E/(k_B T)} - 1}. \quad (15)$$

The heat capacity is then derived from

$$C_P = T \left.\frac{\partial S}{\partial T}\right|_P. \quad (16)$$

Components of the phonon entropy (calculated from the phonon DOS as described previously [13]) are presented in Fig. 10(a). The phonon entropy was calculated from the neutron-weighted DOS at all temperatures and the neutron-weight-corrected DOS at 300 K, which has a somewhat higher ratio of high-energy modes to low-energy modes. The small discrepancy between these two results at 300 K was scaled to other temperatures, assuming the same number of modes in the high-energy and low-energy regions of the phonon DOS. The results are compared to quasiharmonic calculations with a phonon DOS that changes with thermal expansion in the Supplemental Material. The agreement is good at 300 K, but the effect of anharmonicity is to increase the phonon entropy by approximately $0.5\,k_B$/atom at 1050 K, much larger than the estimated electronic contribution.

At 325 K, the phonon contribution to the heat capacity is 25.0 J/(mol K), while the magnetic and electronic contributions are 7.3 and 1.4 J/(mol K) respectively [7]. The majority of the heat capacity comes from the phonons, but the magnetic and electronic parts are not negligible. As the temperature increases, however, the static magnetic order in $FeGe_2$ will disappear and the magnetic heat capacity will decrease to near zero. For example, at 1020 K, the magnetic contribution is almost zero, while the estimated electronic heat capacity is 4.4 J/(mol K) and the phonon heat capacity is 31.6 J/(mol K), as shown in Fig. 10. As a result, phonons contribute a growing fraction of the heat capacity of $FeGe_2$ as the temperature increases (from 74% at 325 K to 87% at 1020 K).

Phonons were also divided into the low- and high-energy parts such that their numbers of states were in the ratio 2:1, approximated by the weights used in Eq. (10). The phonon heat capacities calculated from these two parts are shown separately in Fig. 10(b). The QH model fails to predict the heat capacity for both energy regions, although the gap of the low-energy part is narrowing with temperature.

VI. CONCLUSION

Phonon anharmonicity was studied in paramagnetic $FeGe_2$ between 300 and 1050 K. Inelastic neutron scattering was used to measure the phonon spectrum from a powdered sample from 300 to 1050 K, and ^{57}Fe nuclear resonant inelastic

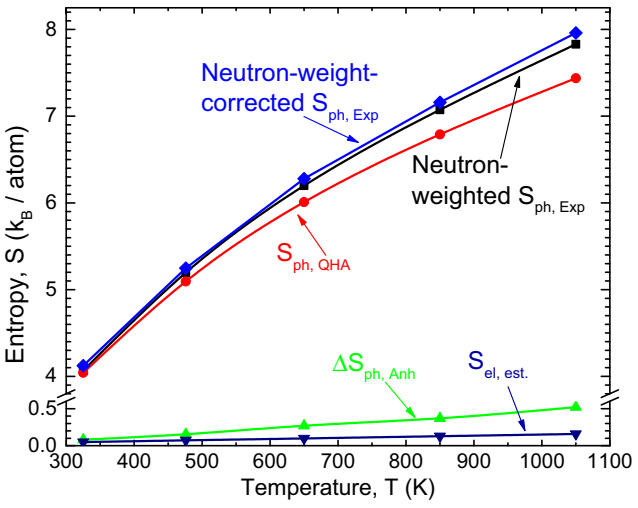

(a)

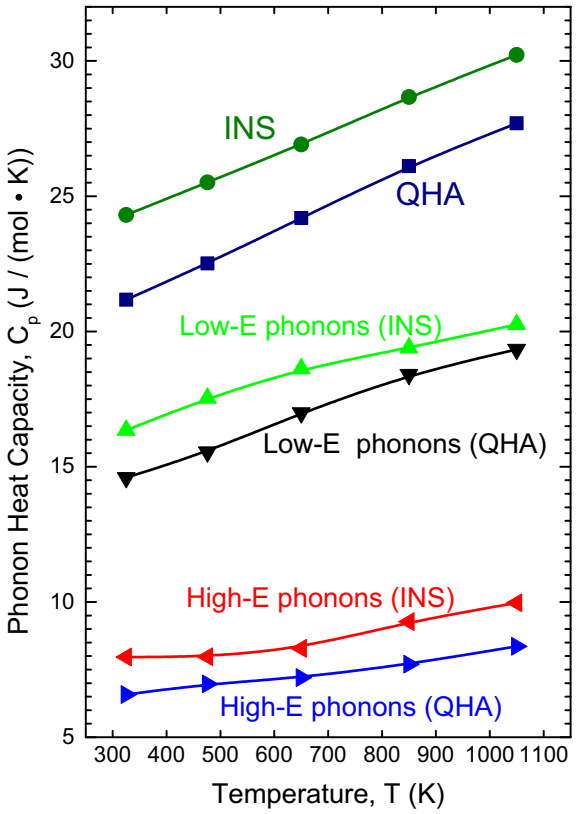

(b)

FIG. 10. Temperature dependence of the entropy in $FeGe_2$ and the phonon contribution to its heat capacity. (a) Components of the entropy [13] of $FeGe_2$ and their temperature dependence. $S_{ph,Exp}$ are from the neutron-weighted (in black) and neutron-weight-corrected (in blue) phonon DOS, respectively. $S_{ph,QHA}$ (in red) are from the calculated phonon DOS using the quasiharmonic approximation. The anharmonic contribution ($\Delta S_{ph,Anh}$, in green) was obtained by $\Delta S_{ph,Anh} = S^{nw-corrected}_{ph,Exp} - S_{ph,QHA}$. The small entropy from electrons ($S_{el,est.}$, in navy) was estimated with $S_{el,est.} = \frac{\pi}{3} k_B T n(\epsilon_F)$, where $n(\epsilon_F)$ is the electronic DOS at the Fermi level in the ground state. (b) Temperature dependence of the phonon contribution to the heat capacity, calculated from measured phonon DOS by the INS experiments and QH approximation. Magnetic contributions, not shown here, are expected at low temperatures.

x-ray scattering was used to measure the partial phonon DOS of ^{57}Fe to correct for differences in the neutron weights for phonon scattering by Fe and Ge. Comparisons with phonon calculations by DFT in the quasiharmonic approximation were successful for the low-energy part of the vibrational spectrum, but the high-energy part showed obvious discrepancies. Thermal shifts of the phonon DOS were measured, and agreed in part with the DFT calculations in the quasiharmonic approximation. There was a modest difference in the average isobaric Grüneisen parameters from computation and experiment, however.

Phonon dispersions were measured by inelastic neutron scattering on a single crystal of $FeGe_2$ at 300, 500, and 635 K. The large number of dispersions made detailed analysis challenging, but some thermal shifts and broadenings of individual phonons were identified. The high-energy phonon dispersions showed more broadening and variations in their thermal shifts than the low-energy modes. Some of this energy shift of high-energy modes could be caused by a cubic anharmonicity to first order, for which the Fe-Ge first-neighbor bond can have an asymmetrical potential in the C16 structure. Nevertheless, the average thermal trends of phonons in $FeGe_2$ do not differ dramatically from the predictions of the quasiharmonic approximation, and this approximation may be useful for understanding some thermophysical properties, even though it does not predict correctly the individual phonon frequency shifts, and of course, the lifetime broadening of the phonon energies. Below 700 K $FeGe_2$ is modestly anharmonic, but the anharmonic contributions were interpretable.

ACKNOWLEDGMENTS

This work was supported by DOE BES under Contract No. DE-FG02-03ER46055. A portion of this research at Oak Ridge National Laboratory's Spallation Neutron Source was sponsored by the Scientific User Facilities Division, Office of Basic Energy Sciences, U.S. Department of Energy. Portions of this work were performed at HPCAT (Sector 16), Advanced Photon Source (APS), Argonne National Laboratory. HPCAT operations are supported by DOE-NNSA under Award No. DE-NA0001974 and DOE-BES under Award No. DE-FG02-99ER45775, with partial instrumentation funding by NSF. The Advanced Photon Source is a U.S. Department of Energy (DOE) Office of Science User Facility operated for the DOE Office of Science by Argonne National Laboratory under Contract No. DE-AC02-06CH11357. This work benefited from DANSE software developed under NSF Grant No. DMR-0520547. Part of the calculations performed herein were made possible by resources of the National Energy Research Scientific Computing Center, a DOE Office of Science User Facility supported by the Office of Science of the U.S. Department of Energy under Contract No. DE-AC02-05CH11231.

[1] S. A. Wolf, D. D. Awschalom, R. A. Buhrman, J. M. Daughton, S. von Molnár, M. L. Roukes, A. Y. Chtchelkanova, and D. M. Treger, Science **294**, 1488 (2001).
[2] K. Yasukochi, K. Kanematsu, and T. Ohoyama, J. Phys. Soc. Jpn. **16**, 429 (1961).
[3] E. Kren and P. Szabo, Phys. Lett. **11**, 215 (1964).
[4] N. S. Murthy, R. Begum, C. Somanathan, and M. Murthy, Solid State Commun. **3**, 113 (1965).
[5] E. Franus-Muir, E. Fawcett, and V. Pluzhnikov, Solid State Commun. **52**, 615 (1984).
[6] A. Menshikov, Y. Dorofeev, G. Budrina, and V. Syromyatnikov, J. Magn. Magn. Mater. **73**, 211 (1988).
[7] L. M. Corliss, J. M. Hastings, W. Kunnmann, R. Thomas, J. Zhuang, R. Butera, and D. Mukamel, Phys. Rev. B **31**, 4337 (1985).
[8] V. V. Tarasenko, V. Pluzhnikov, and E. Fawcett, Phys. Rev. B **40**, 471 (1989).
[9] C. P. Adams, T. E. Mason, E. Fawcett, A. Z. Menshikov, C. D. Frost, J. B. Forsyth, T. G. Perring, and T. M. Holden, J. Phys.: Condens. Matter **12**, 8487 (2000).
[10] H. Zhou, J. Less-Common Met. **171**, 113 (1991).
[11] C. Wolverton and V. Ozoliņš, Phys. Rev. Lett. **86**, 5518 (2001).
[12] J. L. Feldman, L. L. Boyer, P. J. Edwardson, and J. R. Hardy, Phys. Rev. B **40**, 4105 (1989).
[13] Y. Shen, C. W. Li, X. Tang, H. L. Smith, and B. Fultz, Phys. Rev. B **93**, 214303 (2016).
[14] O. Hellman, P. Steneteg, I. A. Abrikosov, and S. I. Simak, Phys. Rev. B **87**, 104111 (2013).
[15] O. Arnold, J. C. Bilheux, J. M. Borreguero, A. Buts, S. I. Campbell, L. Chapon, M. Doucet, N. Draper, R. F. Leal, M. A. Gigg, V. E. Lynch, A. Markvardsen, D. J. Mikkelson, R. L. Mikkelson, R. Miller, K. Palmen, P. Parker, G. Passos, T. G. Perring, P. F. Peterson *et al.* Nucl. Instrum. Methods Phys. Res., Sect. A **764**, 156 (2014).
[16] getdos, http://code.google.com/p/getdos.
[17] R. T. Azuah, L. R. Kneller, Y. Qiu, P. L. W. Tregenna-Piggott, C. M. Brown, J. R. Copley, and R. M. Dimeo, J. Res. Natl. Inst. Stand. Technol. **114**, 341 (2009).
[18] A. Chumakov and W. Sturhahn, Hyperfine Interact. **123**, 781 (1999).
[19] W. Sturhahn and V. Kohn, Hyperfine Interact. **123**, 367 (1999).
[20] W. Sturhahn, Hyperfine Interact. **125**, 149 (2000).
[21] G. Kresse and J. Furthmüller, Comput. Mater. Sci. **6**, 15 (1996).
[22] G. Kresse and J. Hafner, Phys. Rev. B **47**, 558 (1993).
[23] G. Kresse and J. Furthmüller, Phys. Rev. B **54**, 11169 (1996).
[24] G. Kresse and D. Joubert, Phys. Rev. B **59**, 1758 (1999).
[25] J. P. Perdew, K. Burke, and M. Ernzerhof, Phys. Rev. Lett. **77**, 3865 (1996).
[26] A. Togo and I. Tanaka, Scr. Mater. **108**, 1 (2015).
[27] M. S. Lucas, J. A. Muñoz, O. Delaire, N. D. Markovskiy, M. B. Stone, D. L. Abernathy, I. Halevy, L. Mauger, J. B. Keith, M. L. Winterrose, Y. Xiao, M. Lerche, and B. Fultz, Phys. Rev. B **82**, 144306 (2010).
[28] F. C. Yang, O. Hellman, M. S. Lucas, H. L. Smith, C. N. Saunders, Y. Xiao, P. Chow, and B. Fultz, Phys. Rev. B **98**, 024301 (2018).

[29] O. Hellman and I. A. Abrikosov, Phys. Rev. B **88**, 144301 (2013).

[30] D. S. Kim, O. Hellman, J. Herriman, H. L. Smith, J. Y. Y. Lin, N. Shulumba, J. L. Niedziela, C. W. Li, D. L. Abernathy, and B. Fultz, Proc. Natl. Acad. Sci. USA **115**, 1992 (2018).

[31] E. Havinga, H. Damsma, and P. Hokkeling, J. Less-Common Met. **27**, 169 (1972).

[32] See Supplemental Material at http://link.aps.org/supplemental/10.1103/PhysRevMaterials.2.103602 for thermodynamic data including lattice constants and thermal expansion, additional single crystal inelastic scattering results, and calculated phonon spectra at 635 K.

[33] G. E. Grechnev, J. Kubler, and I. V. Svechkarev, J. Phys.: Condens. Matter **3**, 7199 (1991).

[34] D. S. Kim, H. L. Smith, J. L. Niedziela, C. W. Li, D. L. Abernathy, and B. Fultz, Phys. Rev. B **91**, 014307 (2015).

[35] A. A. Maradudin and A. E. Fein, Phys. Rev. **128**, 2589 (1962).